Supplementary Information

Molecular Packing of Pharmaceuticals Analyzed with Paramagnetic Relaxation Enhancement and Ultrafast Magic Angle Spinning NMR

Xingyu Lu[1, §], Yu Tsutsumi[2], Chengbin Huang[1], Wei Xu[1], Stephen R. Byrn[3],
Allen C. Templeton[1], Alexei V. Buevich[1,*], Jean-Paul Amoureux[4, 5, 6, *], and Yongchao Su[1, 3, 7, *]

[1] MRL, Merck & Co., Inc., Kenilworth, New Jersey, 07033, United States

[2] Bruker BioSpin KK., 3-9, Moriya-cho, Kanagawa-ku, Yokohama-shi,
Kanagawa 221-0022, Japan

[3] Department of Industrial and Physical Pharmacy, College of Pharmacy, Purdue University, Indiana 47907, United States

[4] Univ. Lille, CNRS, Centrale Lille, ENSCL, Univ. Artois, UMR 8181-UCCS-Unité de Catalyse et Chimie du Solide, F-59000 Lille, France

[5] Bruker Biospin, 34 rue de l'industrie, F-67166 Wissembourg, France

[6] Riken NMR Science and Development Division, Yokohama, 230-0045 Kanagawa, Japan.

[7] Division of Molecular Pharmaceutics and Drug Delivery, College of Pharmacy, The University of Texas at Austin, Austin, Texas 78712, United States

§ Current Address: Instrumentation and Service Center for Physical Sciences, Westlake University, Hangzhou, Zhejiang, 310024, China

* Corresponding authors: Y.S.: yongchao.su@merck.com; J.-P. A.: jean-paul.amoureux@univ-lille.fr; A.V.B: alexei.buevich@merck.com

Powder X-ray Diffraction

Powder XRD was conducted on a PANalytical X'Pert Pro X-ray diffractometer (PANalytical, USA) with a Cu Kα (λ = 0.15418 nm) radiation source, using a step size of 0.0334° and an integration time of 3 s at room temperature.

Table S1. ^{13}C and ^{1}H chemical shifts of posaconazaole in crystalline (left) and solution (right) state.

	Solid-state NMR			Solution NMR[2]	
^{13}C No.	^{13}C CS (ppm)[1]	^{1}H CS (ppm)*	^{13}C No.	^{13}C CS (ppm)	^{1}H CS (ppm)
2	67.2	3.85	2	69	3.66
3	38.4	2.96	3	38.9	2.61
4	45.4	3.15	4	37.5	2.3
5	82.3	-	5	84.3	-
6	66.5	3.95	6	70.7	3.9
8	151.4	-	8	153	-
9	115.0	6.95	9	115.1	6.78
10	116.9	7.54	10	118.5	6.93
11	145.3	-	11	145.8	-
12	116.9	7.54	12	118.5	6.93
13	115.0	6.95	13	115.1	6.78
14	128.5	-	14	125.4	-
15	158.8	-	15	159	-
16	105.4	7.73	16	104.5	6.85
17	163.2	-	17	162.8	-
18	110.0	7.19	18	111.3	6.82
19	128.2	8.23	19	128.6	7.38
20	56.3	5.05/5.85	20	56	4.58
23	149.7	8.78	23	151	7.79
25	146.4	8.98	25	144.6	8.11
27	49.3	3.46	27	50.6	3.25
28	48.2	3.46	28	49.2	3.36
30	48.2	3.46	30	49.2	3.36
31	49.3	3.46	31	50.6	3.25
34	149.7	-	34	150.7	-
35	116.9	7.54	35	116.6	7.03
36	122.0	9.5	38	123.6	7.43
37	127.9	-	37	125.5	-
38	121.1	8.78	36	123.6	7.43
39	116.9	7.54	39	116.6	7.03
41	153.9	-	41	153.1	-
44	135.1	11.07	44	134.6	7.67
46	65.1	4.73	47	68.9	4.06
47	69.2	4.73	46	63.5	4.02
49	22.2	1.65	49	23.5	1.94
50	9.2	0.34	50	10.7	0.94
51	22.2	2.24	51	21	1.22

* ^{1}H chemical shifts are tentatively assigned.

Table S2. Full [19]F-^{1}H and [1]H-^{1}H inter-nuclear contacts identified in [1]H-detected 2Ds and corresponding distance data derived from X-ray diffraction.[3] Note that a range of [19]F-^{1}H and [1]H-^{1}H proximities are reported here since multiple protons might exist and connect to same carbon atom.

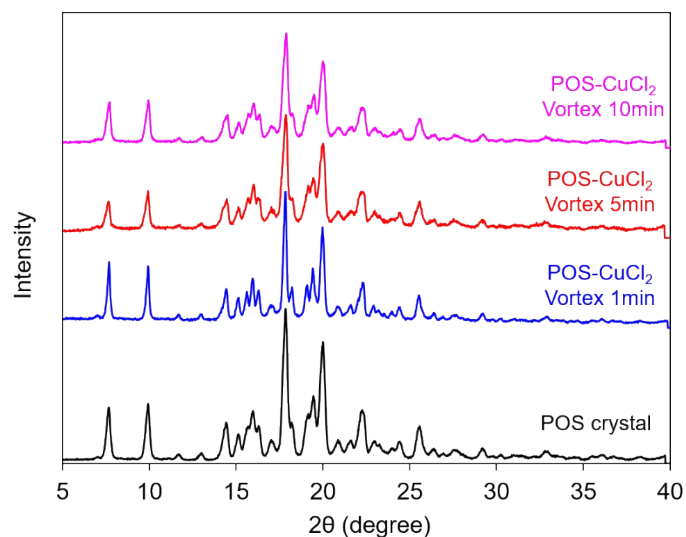| 2D experiments	Spin contacts	Intramolecular	Intermolecular	Inter-nuclear distance from X-ray (Å) [3]
[1]H-^{19}F HETCOR 50 μs contact time $\nu_R = 60$ kHz	[1]H-[19]F	F2-H16		2.53
	[1]H-[19]F	F1-H16		2.55
	[1]H-[19]F	F1-H18		2.53
	[1]H-[19]F		F1-H23	2.43
	[1]H-[19]F		F1-H49/51	3.73-5.29
[1]H-^{19}F HETCOR 1 ms contact time $\nu_R = 60$ kHz	[1]H-[19]F	F2-H18		5.02
	[1]H-[19]F		F1-H46/47	3.45/5.80
	[1]H-[19]F		F1-H50	5.76-6.48
	[1]H-[19]F		F2-H23	5.53
	[1]H-[19]F		F2-H49/51	3.73-5.37
	[1]H-[19]F		F2-H46/47	5.62-5.92
	[1]H-[19]F		F2-H50	4.76-6.02
[1]H-^{1}H RFDR $\nu_R = 60$ kHz	[1]H-[1]H	H50-H49/51		2.32-5.91
	[1]H-[1]H	H50-H46/47		2.53-4.71
	[1]H-[1]H	H49/51-H46/47		2.29-3.51
	[1]H-[1]H	H44-H46/47		4.63-5.00
	[1]H-[1]H	H44-H38		2.31
	[1]H-[1]H		H44-H25	3.74
[1]H-^{1}H RFDR $\nu_R = 110$ kHz	[1]H-[1]H		H50-H3/4	2.40-5.79
	[1]H-[1]H		H50-H2	4.36-6.48
	[1]H-[1]H		H50-H6	4.50-6.41
	[1]H-[1]H	H50-H44		4.18-5.58
	[1]H-[1]H	H49-H51		2.27-4.15
	[1]H-[1]H		H51-H20	4.08-6.25
	[1]H-[1]H		H51-H16	2.78-4.31
	[1]H-[1]H		H51-H25	4.54-5.23
	[1]H-[1]H	H3-H2/H6		2.28-2.83
	[1]H-[1]H	H4-H2/H6		2.46-3.90
	[1]H-[1]H	H3/4-H25		4.52-5.38
	[1]H-[1]H		H3/4-H38	4.8-6.62
	[1]H-[1]H		H3/4-H36	5.35-6.97
	[1]H-[1]H		H6-H36	3.25-3.96
	[1]H-[1]H		H46/47-H20	3.74-6.40
	[1]H-[1]H		H46/47-H16	4.00-5.45
	[1]H-[1]H	H46/47-H38		6.31-6.36
	[1]H-[1]H		H46/47-H25	2.85-4.81
	[1]H-[1]H	H20-H23/25		2.61-4.95
	[1]H-[1]H		H20-H38	6.03-7.18
	[1]H-[1]H	H16-H23/H25		6.64-7.48

Figure S1. PXRD patterns of crystalline POSA without (black) and with (colored) Cu(II) doping on particles surface at different vortex times.
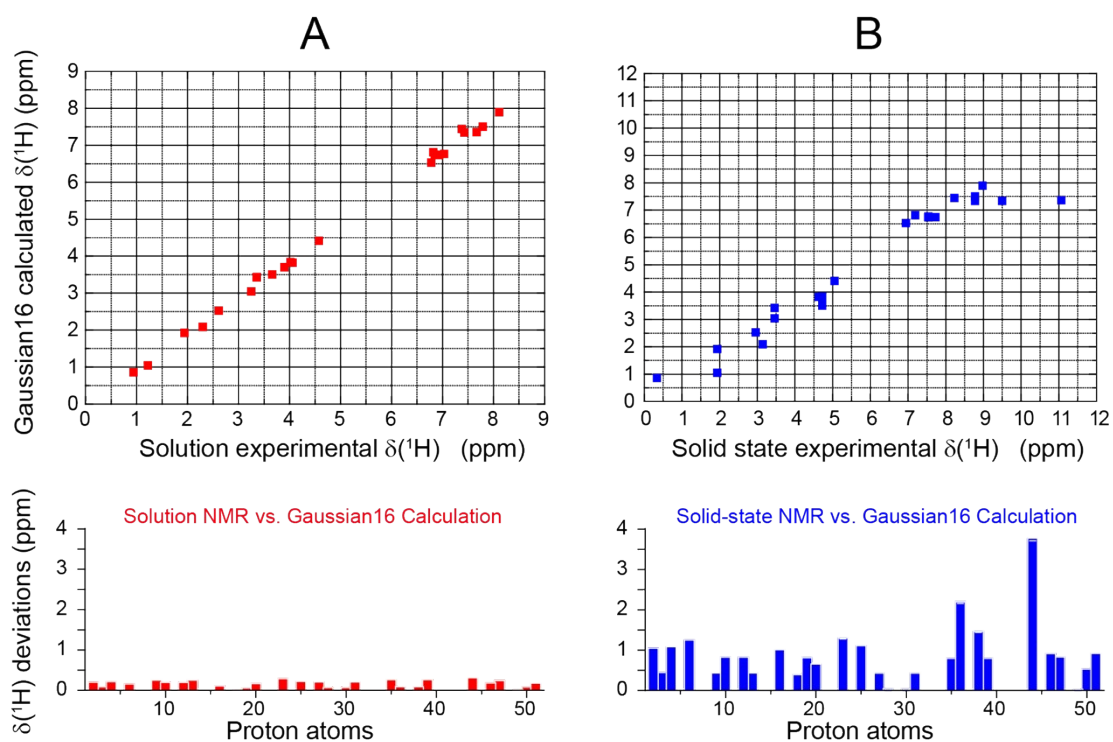

Figure S2. Comparison of ^{1}H chemical shifts in POSA calculated using Gaussian16 with experimental values in solution (A) and solid-state (B).
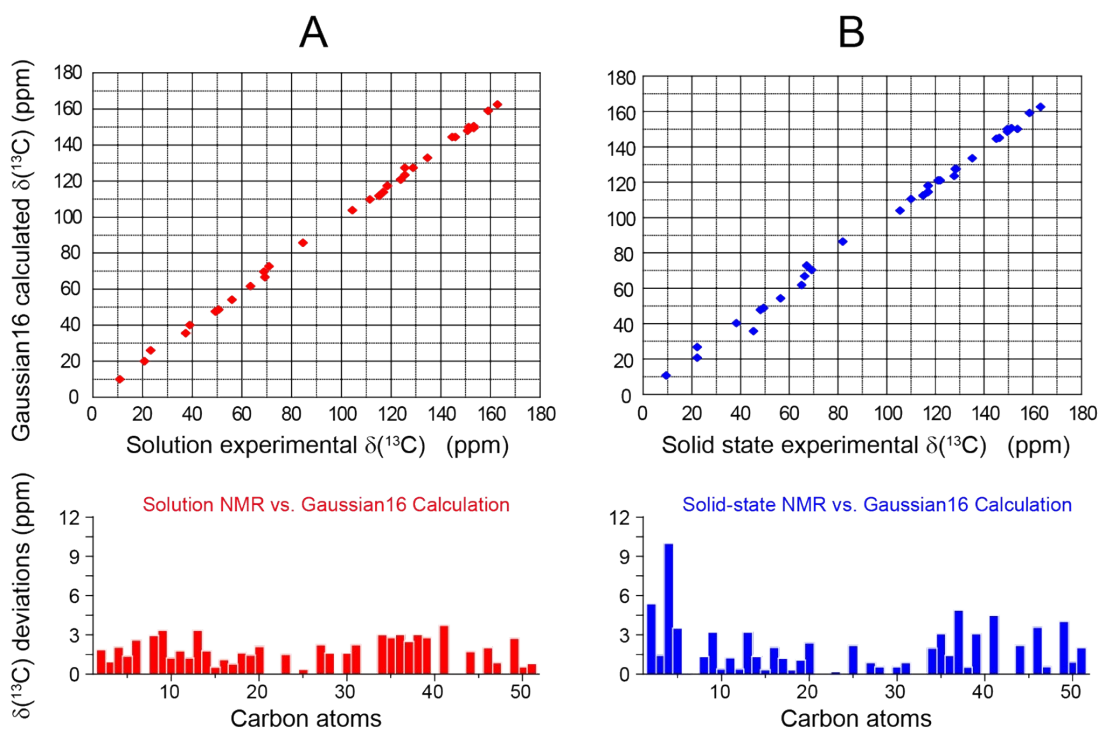
Figure S3. Comparison of ^{13}C chemical shifts in POSA calculated using Gaussian16 with experimental values in solution (A) and solid-state (B).
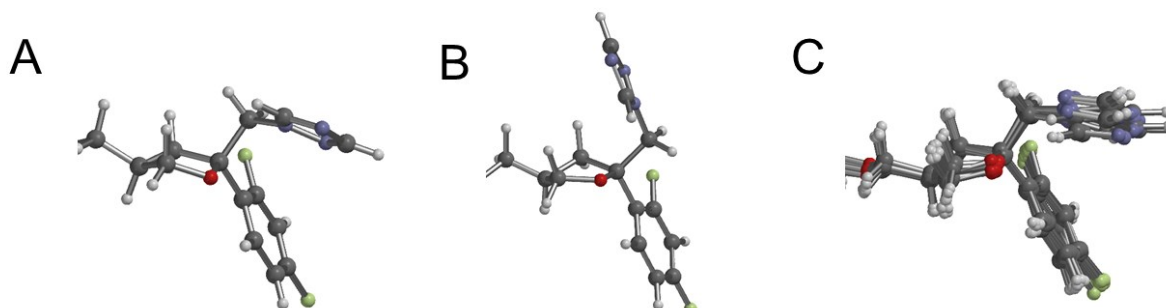

Figure S4. Conformational comparison of the difluorophenyl end of POSA in solid state (A), lowest energy conformation in solution (B) and eight high-energy solution conformations (DE = 3.0- 5.0 kcal/mol) with similar ring orientation to that in the solid state.

Reference

1. Lu, X.; Huang, C.; Li, M.; Skomski, D.; Xu, W.; Yu, L.; Byrn, R. S.; Templeton, C. A.; Su, Y., Molecular Mechanism of Crystalline-to-Amorphous Conversion of Pharmaceutical Solids from ^{19}F Magic Angle Spinning NMR. *J. Phys. Chem. B,* **2020**, https://doi.org/10.1021/acs.jpcb.0c02131

2. Yang, F; Su, Y; Small, J; Huang, C; Martin, G. E; Farrington, A. M.; DiNunzio, J; and Brown, C. D, Probing the Molecular-Level Interactions in an Active Pharmaceutical Ingredient (API) - Polymer Dispersion and The Resulting Impact on Drug Product Formulation, Pharmaceutical Research, **2020**, 37, 94

3. McQuiston, D. K; Mucalo, M. R; and Saunders, G. C, The structure of posaconazole and its solvates with methanol, and dioxane and water: Difluorophenyl as a hydrogen bond donor, Journal of Molecular Structure, **2019**, 1179, 477-486.